HOT H$_2$O EMISSION AND EVIDENCE FOR TURBULENCE IN THE DISK OF A YOUNG STAR

JOHN S. CARR[1]

Naval Research Laboratory, Code 7213, Washington, DC 20375; carr@nrl.navy.mil

ALAN T. TOKUNAGA[1]

Institute for Astronomy, University of Hawaii, 2680 Woodlawn Drive, Honolulu, HI 96822; tokunaga@ifa.hawaii.edu

AND

JOAN NAJITA[1]

National Optical Astronomy Observatory, 950 North Cherry Avenue, Tucson, AZ 85719; najita@noao.edu

ABSTRACT

We report on the detection and analysis of hot rovibrational H$_2$O emission from SVS 13, a young stellar object previously known to have strong CO overtone band head emission. Modeling of the high-resolution infrared spectrum shows that the H$_2$O emission is characterized by temperatures of $\sim$1500 K, significantly lower than the temperatures that characterize the CO band head emission. The widths of the H$_2$O lines are also found to be smaller than those of the CO lines. We construct a disk model of the emission that reproduces the CO and H$_2$O spectrum. In this model, the H$_2$O lines originate at somewhat larger disk radii ($\leq$0.3 AU) than the CO overtone lines ($\leq$0.1 AU). We find that the H$_2$O abundance is about a factor of 10 lower than the calculated chemical equilibrium abundance. Large, approximately transonic, local line broadening is required to fit the profile of the CO band head. If this velocity dispersion is identified with turbulence, it is of significant interest regarding the transport of angular momentum in disks. Large local broadening is also required in modeling CO overtone emission from other young stellar objects, suggesting that large turbulent velocities may be characteristic of the upper atmospheres of the inner disks of young stars.

Subject headings: accretion, accretion disks — circumstellar matter — infrared: stars — planetary systems: protoplanetary disks — stars: formation — stars: pre–main-sequence

1. INTRODUCTION

The presence of hot molecular gas in the circumstellar environment of a number of young stellar objects (YSOs) has been established through observations of first-overtone CO band head emission (Scoville et al. 1983; Thompson 1985; Geballe & Persson 1987; Carr 1989). The CO overtone emission arises from gas with temperatures of $\sim$3000 K and densities $\geq 10^{10}$ cm^{-3}. High-resolution spectroscopy has shown that the shape of the band heads in most objects is consistent with emission from a rotating disk (Carr et al. 1993; Chandler, Carlstrom, & Scoville 1995; Najita et al. 1996). In lower mass YSOs, the emission must originate within a few tenths of an AU from the star. The emission lines are likely to be produced in a temperature inversion in the atmosphere of the accretion disk (Calvet et al. 1991; Najita et al. 1996).

More recent work has concentrated on the fundamental bands of CO (Carr, Mathieu, & Najita 2001; Najita, Carr, & Mathieu 2003; Brittain et al. 2003). Emission in the fundamental bands is detected in most classical T Tauri stars (CTTSs), unlike the situation for the CO overtone bands, which are detected in only a few percent of T Tauri stars. This difference in detection frequency can be attributed to the much higher A-values of the fundamental transitions and the lower energy of the $v = 1$ level, which allow far smaller column densities and lower excitation gas to be detected. The fundamental emission in CTTSs is characterized by typical temperatures of $\sim$1000 K, and the lines are often optically thick. Najita et al. (2003) argue that the emission is most likely to arise in a disk. In contrast to the often strongly double-peaked profiles of the overtone emission, the fundamental profiles are normally centrally peaked. This implies that the emission must extend over a large range in radii, from $\sim$0.04 to $\geq$1 AU based on the velocity widths. Emission from the atmosphere of an optically thick disk is suggested, as for the case of the overtone bands; however, in spectroscopic binaries, where the inner disk is expected to be tidally disrupted, the emission may arise from residual gas in disk gaps.

Molecules other than CO are expected to exist at the temperatures and densities in the inner few AU of disks. Water should be very abundant in the gas phase at temperatures below the dissociation temperature ($\sim$2500 K) and above the water-ice sublimation temperature ($\sim$150 K). In the absence of grains, H$_2$O will be a major coolant and source of opacity. In general, H$_2$O should be an excellent diagnostic of gas within the inner disk because of its high abundance and its rich rovibrational and rotational spectrum in the near- to far-infrared, which can sample a large range in excitation conditions because of the wide range of energy levels and line strengths. While cool water vapor ($<$500 K) is difficult to observe from the ground because of telluric absorption, hot water is easily studied. The detection of emission from hot H$_2$O has already been reported from some YSOs known to have CO overtone emission (Najita et al. 2000). In this paper, we present and discuss in detail the detection of H$_2$O emission from SVS 13, a

Report Documentation Page

1. REPORT DATE **2004**	2. REPORT TYPE	3. DATES COVERED **00-00-2004 to 00-00-2004**

4. TITLE AND SUBTITLE	5a. CONTRACT NUMBER
Hot H2O Emission and Evidence for Turbulence in the Disk of a Young Star	5b. GRANT NUMBER
	5c. PROGRAM ELEMENT NUMBER

6. AUTHOR(S)	5d. PROJECT NUMBER
	5e. TASK NUMBER
	5f. WORK UNIT NUMBER

7. PERFORMING ORGANIZATION NAME(S) AND ADDRESS(ES) **Naval Research Laboratory,Code 7213,4555 Overlook Avenue, SW,Washington,DC,20375**	8. PERFORMING ORGANIZATION REPORT NUMBER

9. SPONSORING/MONITORING AGENCY NAME(S) AND ADDRESS(ES)	10. SPONSOR/MONITOR'S ACRONYM(S)
	11. SPONSOR/MONITOR'S REPORT NUMBER(S)

12. DISTRIBUTION/AVAILABILITY STATEMENT
Approved for public release; distribution unlimited

13. SUPPLEMENTARY NOTES

14. ABSTRACT

15. SUBJECT TERMS

16. SECURITY CLASSIFICATION OF:			17. LIMITATION OF ABSTRACT	18. NUMBER OF PAGES **8**	19a. NAME OF RESPONSIBLE PERSON
a. REPORT **unclassified**	b. ABSTRACT **unclassified**	c. THIS PAGE **unclassified**			

YSO known to have prominent CO overtone band head emission.

2. OBSERVATIONS

High-resolution spectra of SVS 13 were obtained at the NASA Infrared Telescope Facility (IRTF) using CSHELL, the facility cryogenic infrared echelle spectrograph (Tokunaga et al. 1990; Greene et al. 1993), which is equipped with a 256×256 SBRC InSb array. The observations were made on 1994 November 13 UT. CSHELL uses order-sorting filters to isolate a single echelle order; for these observations, we used a custom narrowband wedged filter, centered at 2.32 μm, that eliminates the channel fringing that was normally seen with the circular variable filters. Two overlapping grating settings centered near 2.293 μm were obtained. The $1''$ slit was used, giving a 5 pixel resolution $R = 23,000$. For flux calibration, a short exposure of both SVS 13 and HD 18881 ($K = 7.140$) were obtained through a $4''$ wide slit. In the normal observing procedure, the telescope is nodded between integrations to place the star at two different positions along the slit, and these images are differenced during data reduction to remove dark and background. The extracted spectra of SVS 13 were divided by those of a hot star observed at the same air mass in order to correct for telluric absorption features. The telluric features in the hot-star spectrum were used for wavelength calibration. The resulting telluric-corrected and flux-calibrated spectrum is shown in Figure 1.

A low-resolution ($R = 200$) spectrum of SVS 13 was obtained at the IRTF using SpeX (Rayner et al. 2003) with a prism covering the 0.8–2.5 μm spectral region. The observations were made on 2001 November 1 UT. HD 19600 (spectral type A0 V) was observed as a standard star. The atmospheric absorption and instrumental throughput were obtained by the method described by Vacca, Cushing, & Rayner (2003). The resulting spectrum of SVS 13 is shown in the top panel of Figure 2.

3. RESULTS

The CSHELL spectrum in Figure 1 shows prominent emission from the CO $v = 2-0$ band head, as was first reported by Carr (1989) and subsequently observed at high
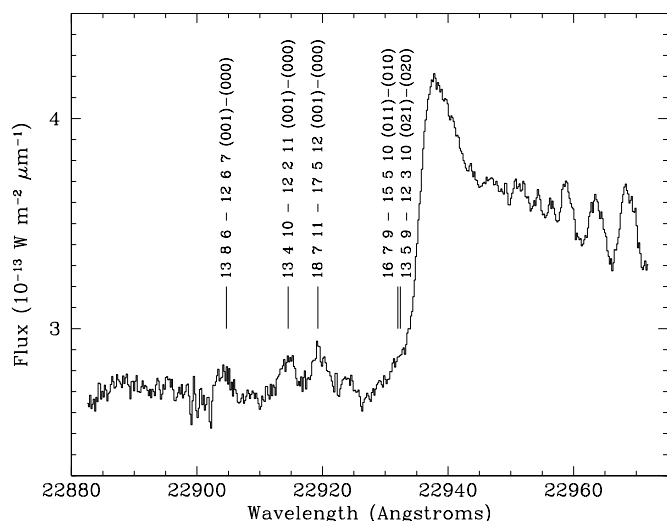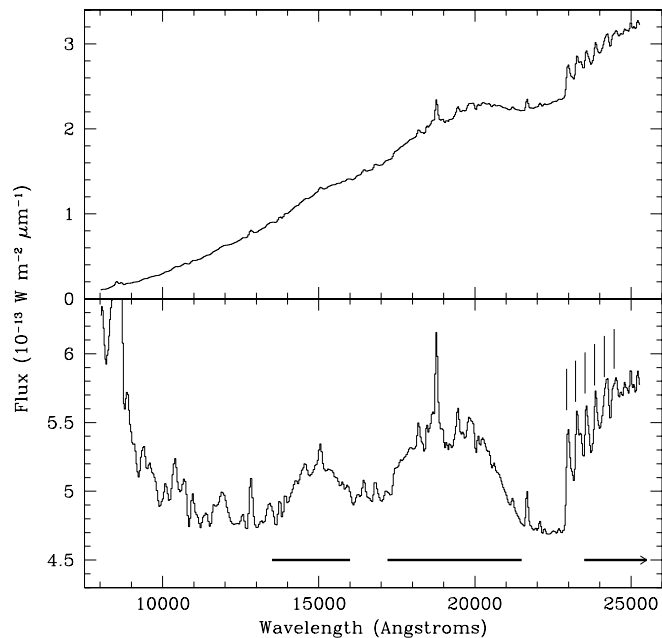

Fig. 2.—*Top*: Low-resolution 0.8–2.5 μm SpeX spectrum of SVS 13. *Bottom*: The same spectrum dereddened (for $A_K = 0.8$) in order to emphasize the H_2O emission bands, whose positions are indicated by the thick horizontal lines. The positions of the first-overtone CO band heads are marked by the vertical lines.

resolution by Carr & Tokunaga (1992) and Chandler et al. (1993). Significant spectral structure is also observed at wavelengths blueward of the CO band head ($\lambda < 2.2935$ μm). The strongest of these emission features were found to correspond in wavelength with absorption lines of H_2O that have been identified by Zobov et al. (2000) in sunspot spectra. The line assignments of Zobov et al. are marked in Figure 1. The H_2O emission also appears to contribute to the blue wing of the CO band head. Given the identification of the emission lines with high rotational transitions that are also observed in sunspot spectra, the water emission must originate from hot gas.

The presence of H_2O emission is corroborated by the low-resolution SpeX spectrum. In the bottom panel of Figure 2, we show the spectrum of SVS 13 dereddened in order to flatten and clearly show the entire 1.0–2.5 μm spectrum. Broad emission features are seen that correspond to the H_2O bands at 1.4, 1.9, and 2.7 μm (the latter is blended with CO). These same bands are observed, in absorption, in the spectra of late-type stars.

4. MODELING

We have modeled the high-resolution spectrum of SVS 13 in order to determine the properties of the hot H_2O gas and understand the relation between the H_2O and CO overtone emission. We first describe the construction of an H_2O line list for this purpose, using a combination of theoretical line lists and empirical modeling. We then model the H_2O and CO spectrum, first as emission from gas in a uniform slab and then as emission from a Keplerian disk.

4.1. H_2O Line List

The main difficulty encountered in modeling the spectrum of hot water is the availability of a complete and accurate H_2O line list. One of the more extensive line lists suitable for our

Fig. 1.—High-resolution CSHELL spectrum of SVS 13 in the region of the $v = 2 - 0$ CO band head. The H_2O line assignments for the sunspot spectrum from Zobov et al. (2000) are labeled.

purpose is the theoretical list calculated by Partridge & Schwenke (1997, hereafter PS), which has been used in the most recent generation of atmospheric models for M dwarfs and brown dwarfs (Allard, Hauschildt, & Schweitzer 2000; Allard, Hauschildt, & Schwenke 2000; Allard et al. 2001). However, neither the positions nor strengths of individual lines in the PS list are accurate enough for synthesis of high-resolution spectra. Therefore, we took a semiempirical approach, beginning with the PS list and modeling the H$_2$O lines in a solar sunspot spectrum.

We used a recent version of the stellar synthesis program MOOG (Sneden 1973) and the infrared sunspot spectrum of Wallace & Livingston (1992). The MOOG code was modified to handle the triatomic molecule H$_2$O, using the partition function from Irwin (1988) corrected for the different treatment of the nuclear spin statistical weight. A comparison of the Irwin partition function with that calculated from the PS energy levels showed that the Irwin fit is accurate to better than 1% down to a temperature of 500 K.

The PS list contains about 450,000 lines in the 2.288–2.297 μm wavelength region covered by our high-resolution spectrum of SVS 13. In order to make the list manageable for spectral modeling, we restricted the list to lines with strength greater than 1% of the strongest line in the region (at 22918 Å) at a temperature of 3000 K. This leaves about 350 lines. We also produced lists with cutoffs of 0.1% and 0.01% of the strongest line, and lists using a 1% cutoff at 1000 and 2000 K, in order to investigate the effects of the choice of cutoff threshold and temperature. We next took the line assignments for the solar sunspot spectrum and a laboratory emission spectrum by Zobov et al. (2000) and substituted the observed wavelengths for the corresponding transitions in the PS list. While these line assignments cover very few of the H$_2$O lines in the sunspot spectrum, many of the strongest absorption lines in our wavelength region appear to be identified.

The adjustment of oscillator strengths for individual water transitions is the next issue to address. One approach is to match synthetic spectra to observed high-resolution spectra of an M dwarf or sunspot. We ruled out M dwarfs because of the lack of well-determined abundances and uncertainty in the effective temperatures. One difficulty with sunspots is deciding on the atmospheric structure that accurately represents the observed sunspot. We used the NextGen model structures (Hauschildt, Allard, & Baron 1999) with solar metallicity and $\log g = 4.5$. An abundance analysis of the CO overtone lines was used to determine the effective temperature that best corresponds to the Wallace & Livingston sunspot spectrum. An effective temperature of 3900 K gave a carbon abundance [$\log \epsilon(C) = 8.64$, using the notation $\log \epsilon(C) = \log (C/H)+12.0$] that was roughly independent of line excitation potential and close to the solar photospheric value. Even if this model is not a precise match to the observed sunspot, it should be close enough to adjust the *relative* oscillator strengths of H$_2$O lines. However, this approach may not be sufficient to set the *absolute* oscillator strengths of the lines, because the H$_2$O abundance is highly sensitive to the temperature structure.

To calibrate the absolute oscillator strengths, we used experimental line strengths taken from the HITRAN database (Rothman et al. 1998). Because none of the identified H$_2$O lines in the wavelength region of the SVS 13 spectrum are in the HITRAN list, we used a wavelength region near 23110 Å, where several lines assigned by Zobov et al. (2000) appear in HITRAN. The gf-values for these lines, converted from the

HITRAN line strengths, were substituted into the PS list. We then produced synthetic spectra using the above model and C abundance and adjusted the O abundance to give the best fit to four clean HITRAN H$_2$O lines [the solar value $\log \epsilon(O) = 8.93 \pm 0.04$ gave the best fit]. All four of these lines are from the 001–000 band, and the HITRAN-based gf-values were 1.17–1.35 times greater than the theoretical values in the PS list. We next synthesized sunspot spectra for the region covered by the SVS 13 spectrum, with the C and O abundances fixed, and adjusted the gf-values of the lines identified by Zobov et al. to fit the observed line strengths. These adjustments required an increase of the theoretical gf-values by factors ranging from 1.1 to 2.7; the changes in gf-values for only the 001–000 band lines were 1.1–1.5 times, similar to the ratio of the HITRAN to PS gf-values in the 23110 Å region. With this procedure, we believe that the absolute gf-values for the identified lines are good to 25% and that the relative gf-values are good to 10%.

Figure 3 shows the observed and synthetic sunspot spectra for the wavelength region blueward of the CO band head. The H$_2$O line at 22913 Å could not be fitted because of strong telluric absorption; the gf-value for this line was set to 1.3 times the PS theoretical value, which is the median ratio of empirical to theoretical gf-values for the other 001–000 lines. There are some prominent lines in the sunspot spectrum (22882, 22892, and 22908 Å) that are not accounted for. However, emission centered at these wavelengths is clearly not present in the SVS 13 spectrum. These absorption lines could be due to a molecule other than H$_2$O or to higher excitation H$_2$O transitions that are not populated in the (presumably cooler) circumstellar gas of SVS 13. The theoretical line list also leaves significant opacity due to moderate strength lines unaccounted for (e.g., near 22887 and 22929 Å). The inadequacy of current theoretical H$_2$O line lists is a general problem that also reveals itself in the spectral modeling of late-type stars at low resolution (Allard et al. 2000b; Leggett et al. 2000, 2001; Jones et al. 2002). In order to check that our reduced line list is not missing important
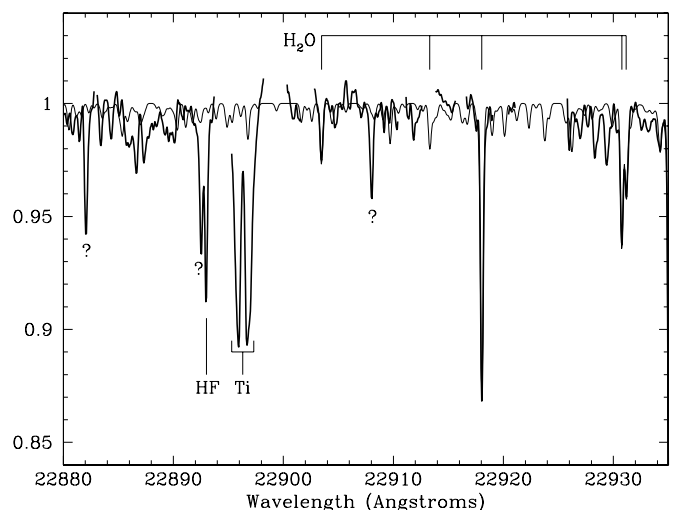

F$_{IG}$. 3.—Observed sunspot spectrum (*thick line*) from Wallace & Livingston (1992) and synthetic spectrum (*thin line*) calculated as described in the text. The positions of assigned H$_2$O lines shown in Fig. 1 are indicated. A question mark labels the strongest unidentified absorption lines. Also labeled are a line of HF and a Zeeman-split Ti I line (neither are included in the synthesis). Wavelength regions with the strongest telluric absorption are not plotted in the observed spectrum.

opacity, we ran the same model using our line lists with cutoffs of 0.1% and 0.01% of the strongest line. The 0.1% cutoff list introduces a veil of very weak lines that depresses the continuum by 0.5% but does not produce any additional spectral features. Use of the line list with a 0.01% cutoff produces no further change. The line lists that were constructed with cutoffs based on temperatures of 1000 and 2000 K gave similar results, except that the lower temperature line lists missed some weak high-excitation lines.

4.2. *Slab Model*

We begin with a simple model with gas of constant temperature, column density Σ, and number density. The gas is assumed to be in chemical equilibrium, and the computation of the chemical equilibrium abundances, which depends only on the local number density and temperature, included all important C and O bearing molecules. In addition, LTE was assumed. Continuum opacity was not included. The gas has a local line profile composed of both a thermal and a nonthermal component. The nonthermal component is characterized by a velocity dispersion ξ ($\Delta V_{\rm FWHM} = 2.355\xi$), with either a Gaussian or Lorentzian profile. A Gaussian macrobroadening is also included to represent bulk gas motions on scales larger than the photon mean free path. The instrumental broadening is a Gaussian with a 13 km s^{-1} FWHM velocity. For this modeling, we sought to match the relative shape and line ratios of the emission; hence, the data were normalized to a continuum level of one, and the model spectra were scaled to match the integrated emission flux of either the CO or H$_2$O.

First, we fitted the CO 2–0 band head using a list with only CO lines. The shape of the band head is very much affected by the overlap of the CO lines and the line optical depth. We found that solutions where the CO lines are optically thin cannot fit the shape of the band head, regardless of the temperature, because the model is too sharply peaked at the band head (22938 Å). Models where the local line profile includes only thermal broadening do not fit for any combination of temperature and column density; such a model also results in a band head that is too sharply peaked with too little flux at wavelengths longer than 22945 Å. The necessity of superthermal local line widths was also found when fitting the CO band head emission from other YSOs (Najita et al. 1996); the line broadening is discussed in § 5. Acceptable fits could be found over the temperature range of 1500–3500 K, which reflects the fact that the CO 2–0 band head, by itself, is more sensitive to optical depth and line broadening than to temperature. As an example of a good fit, at 2000 K, $\Sigma = 8.0$ g cm^{-2} and $\xi = 10$ km s^{-1} (Gaussian), with a macrobroadening of 38 km s^{-1} (FWHM). These parameters give $\tau = 0.5$ in the 2–0 $R(51)$ line. Alternately, a similar fit can be obtained using a Lorentzian nonthermal profile with $\xi = 2.8$ km s^{-1} and $\Sigma = 12$ g cm^{-2}. In general, different shapes for the local line profile give similar results because the bulk gas motions dominate the total line broadening.

Next, we fitted the H$_2$O lines blueward of the band head using only H$_2$O lines, but we added to the model the previous 2000 K CO model in order to account for the contribution of the CO band head wing near 22933 Å. The density was set sufficiently high (10^{12} cm^{-3}) that H$_2$O has its maximum chemical equilibrium abundance. The H$_2$O lines with calibrated line strengths have a range in excitation potential of 0.3–0.6 eV and hence provide some diagnostic of the gas temperature. A temperature of $\sim$1500 K worked best, while $T = 1000$ K gave an inadequate fit and 2000 K was definitely

too hot. We found that different combinations of ξ and Σ gave similar results because overlap of the main H$_2$O lines is not important, unlike the case for the CO band head. In all cases, optically thick H$_2$O lines provided a better fit than optically thin lines. For example, a reasonable fit at 1500 K is achieved with $\Sigma = 9.0$ g cm^{-2} (giving $\tau = 6.0$ in the 22918 Å line), $\xi = 10$ km s^{-1} (Gaussian), and a macrobroadening of 21 km s^{-1}. This model is shown in the top panel of Figure 4 (*smooth solid line*) overplotted on the observed spectrum. The apparent wing to the CO band head at 22931 Å is fitted well with the inclusion of the H$_2$O emission. This wing could not be fitted with the CO models in Chandler et al. (1995) and Carr & Tokunaga (1992). Note that the line broadening for the H$_2$O lines is significantly less than for the CO band head. This is illustrated by the dotted line in the top panel of Figure 4, which is the same H$_2$O model but with the 38 km s^{-1} macrobroadening that was required for CO.

The best temperature of $\sim$1500 K is much lower than the 3000 K used to determine the cutoff threshold in our main line list. Therefore, we ran one test case for the above 1500 K model using the line list constructed for 1000 K. Some additional low-excitation lines are present in the 1000 K list, but these lines do not produce any significant difference in the model spectrum.

For a slab model, we find that there is no set of parameters that can simultaneously fit the H$_2$O and CO emission. The first, and obvious, difficulty is that the H$_2$O lines are narrower than the CO lines (Fig. 4, *top*). The second problem lies in the

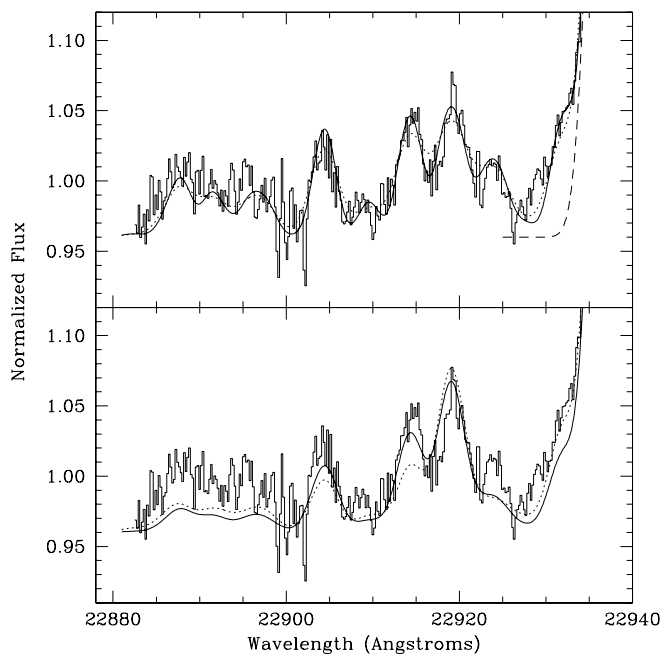Fig. 4.—*Top*: Slab model (*smooth solid line*) that provides a good fit to the H$_2$O emission lines. The parameters for the model are $T = 1500$ K, $\Sigma = 9.0$ g cm^{-2}, $\xi = 10$ km s^{-1}, and a Gaussian macrobroadening of 21 km s^{-1}. The H$_2$O lines are optically thick. The dashed line shows the contribution due to CO alone. The dotted line is the same model but with the macrobroadening of 38 km s^{-1} that best fits the CO band head, illustrating the different broadenings for the CO and H$_2$O lines. *Bottom*: Models that fit the CO band head compared to the observed H$_2$O lines, after adjusting the number density to change the H$_2$O chemical equilibrium abundance and match the relative CO to H$_2$O fluxes. The solid line is for $T = 1500$ K, $\Sigma = 8.0$ g cm^{-2}, $\xi = 10$ km s^{-1}, and a Gaussian macrobroadening of 38 km s^{-1}. The H$_2$O lines are now optically thin, and the fit is not as good as the solid line in the top panel. The dotted line is for $T = 2000$ K and $\Sigma = 10.0$ g cm^{-2}.

gas temperature. The H$_2$O emission indicates a temperature of $\sim$1500 K. This temperature is at the low end of the range that can fit the CO 2–0 band head; however, a temperature this low for the CO emission can be ruled out by the presence of emission from higher vibrational band heads (e.g., $v = 5{-}3$), which requires gas temperatures of $\geq$2500 K (Carr 1989). In addition, too much H$_2$O emission is produced at 1500 K relative to CO, and the H$_2$O column density must be reduced substantially to match the relative flux. This can be done by reducing the number density and hence the H$_2$O chemical equilibrium abundance. However, the H$_2$O lines then become optically thin ($\tau_{22918} = 0.27$), and the resulting fit to the H$_2$O line ratios is poorer (Fig. 4, *bottom, solid line*). Higher gas temperatures do not improve the situation. The bottom panel of Figure 4 also shows a model (*dotted line*) with parameters that fit the CO band head for $T = 2000$ K, where the number density is again adjusted to fit the relative H$_2$O to CO flux. The optical depth is still too low ($\tau_{22918} = 0.36$), and while the higher temperature helps with the 22931 Å feature, the other line ratios are worse. We conclude that a single slab of uniform gas cannot produce both the H$_2$O and CO emission and that a range of temperatures and line widths is required.

4.3. *Disk Model*

Because a disk model works well for the CO band head emission in many YSOs (Carr et al. 1993; Chandler et al. 1995; Najita et al. 1996), this is a logical model to explore for the H$_2$O emission. H$_2$O has a lower dissociation temperature than CO; therefore, a disk with an outwardly decreasing temperature gradient will naturally give H$_2$O emission lines with smaller line widths and lower excitation temperatures, compared to the overtone CO emission.

In this LTE disk model (see Najita et al. 1996; Carr et al. 2001), the molecular emission arises from a line-emitting layer that is uniform in the vertical direction and whose radial variation of temperature and surface density Σ are specified by power laws. This line-emitting layer may be a temperature inversion in the upper atmosphere of an optically thick disk, or it could correspond to the entire surface density of an optically thin portion of the disk. The chemical equilibrium abundances are calculated as in the slab model, but in this case the average number density comes from the surface density and the thickness of the layer, taken as the pressure scale height in hydrostatic equilibrium. The local line broadening is treated the same as in the slab model, but now all macrobroadening is determined by the Keplerian rotation of the disk. The other quantities that must be specified are $v \sin i$ at the inner emission radius, the inner and outer radius of the emission, and the mass of the star; the inclination follows from these parameters. Because we first concentrate on fitting the shape of the CO band head and the width and ratios of the H$_2$O lines, the relevant parameters are the temperature and surface density laws, $v \sin i$, and the *ratio* of the outer to inner *emission* radii, $R_{\rm out}/R_{\rm in}$. The stellar mass has only a minor effect on the model; we take 2 $M_\odot$ based on the bolometric luminosity of SVS 13. The absolute value of the radius is not critical except when fitting the absolute observed flux, in which case the distance and extinction are also required. We will consider the absolute flux after first exploring the parameters required to fit the spectral shape.

The results of the slab modeling provide a guide to the average conditions that are required to fit the data. Because of the many adjustable parameters in the disk model, unique solutions are not possible. Instead, we present a model that is

illustrative of solutions that provide a good match to the observed spectrum. This model has the following parameters: $T = 4000(r/R_{\rm in})^{-0.4}$ K, $\Sigma = 12(r/R_{\rm in})^{-0.4}$ g cm^{-2}, $\xi = 11$ km s^{-1}, $v \sin i = 48$ km s^{-1}, and $R_{\rm out}/R_{\rm in} = 22$. For a Lorentzian local profile, $\Sigma = 22(r/R_{\rm in})^{-0.4}$ g cm^{-2} and $\xi = 3.2$ km s^{-1} give an equivalent result. The exponents for the temperature and surface density power laws are arbitrary but plausible values. The values for Σ, ξ, and $v \sin i$ were set by fitting the shape of the CO band head, while $R_{\rm out}/R_{\rm in}$ was set to provide the correct average temperature for the H$_2$O gas. The temperature at the outer radius is 1160 K, and $\Sigma = 3.5$ g cm^{-2}.

A possible physical interpretation for an outer cutoff in emission at this radius and temperature is the presence of dust in the upper atmosphere. The temperature at the outer radius is very close to the grain vaporization temperature (Pollack et al. 1994) for the model number density of 5×10^{11} cm^{-3} at this radius. Using the Rosseland mean opacities from Henning & Stognienko (1996), the continuum optical depth due to dust in the layer would be $\tau = 20$. This is high enough to effectively suppress the molecular line emission.

Figure 5 shows this model when the flux is scaled to match the observed flux in the CO band head. The solid line in Figure 5 is the model spectrum using only CO lines. When the H$_2$O lines are added to the synthesis, it is found that the H$_2$O line flux, relative to CO, is far too large. The molecular abundances in chemical equilibrium are set by the temperature and number density at each radius. It is not possible to independently vary the number density, as was done in the slab model, because the number density is set by the surface density, temperature, and pressure scale height for the gas layer. Instead, we allow the H$_2$O abundance to be decreased by an arbitrary amount below its chemical equilibrium value. The dashed line in Figure 5 shows such a model, where the H$_2$O abundance is scaled (by a factor of 0.14) to fit the wing to the CO band head.

In Figure 6 we show the *same* baseline disk model (*solid line*), but scaled instead to the flux under the H$_2$O lines between 22913 and 22922 Å. This model gives a reasonable match to the H$_2$O line width, temperature, and optical depth, although a somewhat better fit (similar to the slab model in the top panel of Fig. 4, *solid line*) would result by increasing Σ by
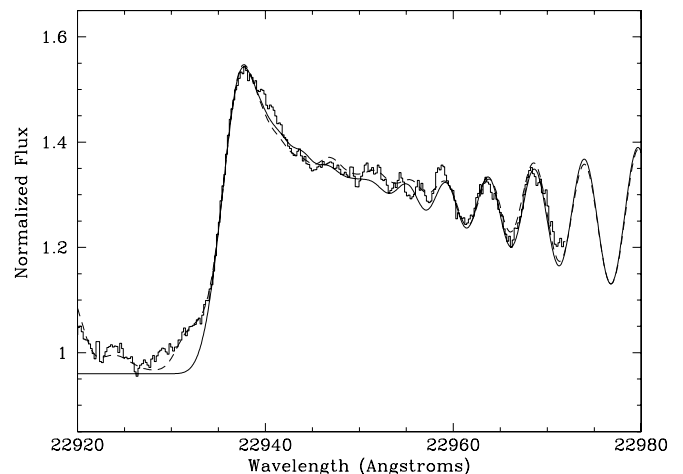

Fig. 5.—Baseline disk model described in the text compared to the CO 2–0 band head in SVS 13 (*histogram*). The solid line is the disk model with only CO lines included, scaled to the flux under the CO band head. The dashed-line includes the H$_2$O lines, with the H$_2$O abundance decreased by 0.14 from its chemical equilibrium value to match the wing at 22933 Å.
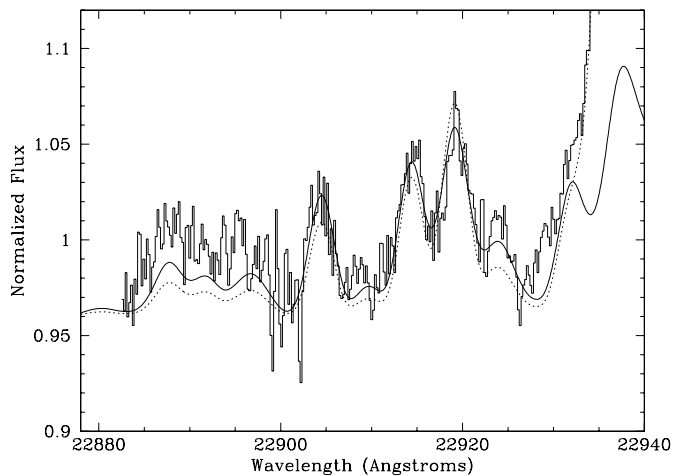
Fig. 6.—Disk models and observed H_2O lines in SVS 13 (*histogram*) shortward of the CO band head. The smooth solid line is the baseline disk model scaled to the flux under the H_2O lines, where the H_2O abundance is set to its chemical equilibrium value. The dotted line is the baseline model scaled to the flux under the CO band head, but the H_2O abundance is decreased from its chemical equilibrium value to fit the average H_2O flux. With the lower abundance, the H_2O lines are optically thin and the fit to the spectrum is not quite as good.

a factor of 2. However, when scaled to the H_2O flux, the model CO emission is now far too weak, as is seen by the low CO flux at 22937 Å (*solid line*). The dotted line in Figure 6 shows the synthetic spectrum when the model is scaled to the CO band head and the H_2O abundance is reduced. This model is identical to the dashed line in Figure 5, expect that the H_2O abundance is scaled to match the H_2O flux between 22913 and 22922 Å rather than the wing at 22931 Å. This result is similar to the problem encountered when reducing the H_2O abundance in the slab model: decreasing the H_2O column density to match the relative H_2O and CO fluxes produces optically thin H_2O lines that give a poorer match to the H_2O line ratios. This may indicate that our disk model is too simple (see discussion in § 5). However, some caution must be exercised regarding our findings about the H_2O optical depth (and excitation temperature) because of the relatively small number of H_2O lines used in the analysis. More definitive conclusions would be provided by an analysis of a far larger number of lines.

Next, we examined the physical radius of the emission that is required to fit the absolute CO flux level in the spectrum. For the distance to SVS 13, we take 350 pc (Herbig & Jones 1983). The extinction is an important but not well-determined factor. The infrared color-color plots in Aspin & Sandell (1997) suggest an extinction in the range of $A_V = 15-25$, or $A_K \sim 2$. If we set $R_{in} = 3.0 \, R_\odot$, for example, then $A_K = 2.05$ ($A_V = 19$) is required to match the CO band head flux. The inclination is $i = 8°$ for this combination of radius, stellar mass, and $v \sin i$. The H_2O emission in this model would extend out to ~0.3 AU. If the extinction is $A_V = 25$ ($A_K = 2.7$), near the upper end of this range, then a radius of $R_{in} = 4.0 \, R_\odot$ is needed, and the emission would extend to ~0.4 AU; R_{in} could be larger by a factor of a couple if the maximum gas temperature in the model is decreased. Regardless of the exact values of the input parameters, the observed CO flux requires the emission region to be rather small, with the inner edge within a few stellar radii of the star.

Figure 7 shows where the CO and H_2O emission are produced in the baseline disk model as a function of radius.

The CO and H_2O emission come from overlapping but largely different parts of the disk. The inner radii are determined by molecular dissociation. The power-weighted average temperatures for the CO and H_2O emission are 2770 and 1680 K, respectively. The typical values of $v \sin i$ are 31 and 17 km s^{-1} for CO and H_2O, respectively.

5. DISCUSSION

We have shown, using both low- and high-resolution spectra, that emission from hot H_2O is present in SVS 13. After constructing an H_2O line list suitable for modeling high-resolution spectra, we modeled both the CO band head and H_2O emission. The velocity widths of the H_2O emission lines are narrower than those for the CO emission, and the H_2O excitation temperature of ~1500 K is significantly lower than the temperature (≥2500 K) required to produce CO emission from high vibrational levels. We constructed a model of emission from a Keplerian accretion disk that naturally provides the correct temperatures and line widths for both the CO and H_2O emission and gives a reasonable match to the observed shape of the CO and H_2O spectra. In this disk model, the peak of the H_2O emission lies at a larger radius than the CO emission (Fig. 7), extending to ~0.3 AU from the star, compared to ~0.1 AU for the CO overtone emission.

In the baseline disk model, the molecular abundances at each disk radius were determined assuming chemical equilibrium. However, we found that the H_2O abundance must be substantially reduced below this value, by a factor of 10, in order to match the H_2O emission flux relative to CO. Strong incident radiation on the disk surface may be responsible for producing molecular abundances that differ from expected equilibrium values. Photodissociation from UV photons is likely to be important near the disk surface, and strong Lyα emission could preferentially destroy some molecules, such as
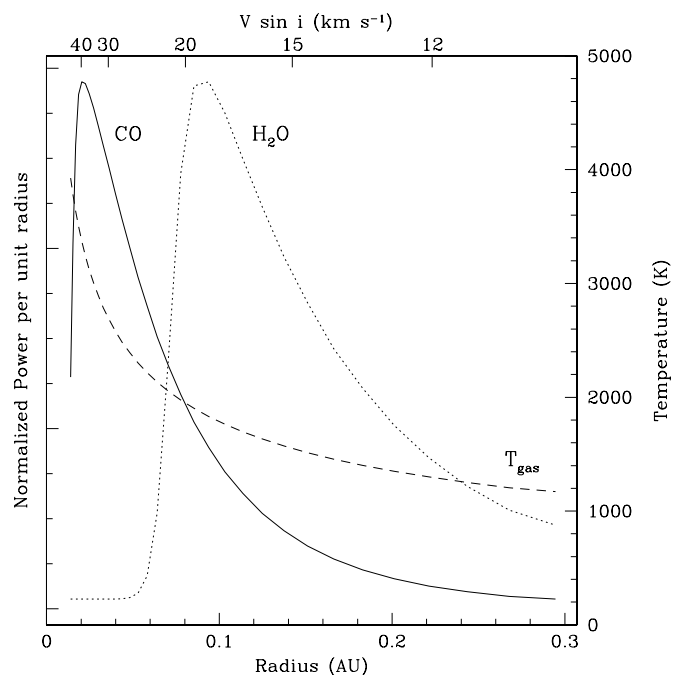

Fig. 7.—Normalized power per unit radius for CO (*solid line*) and H_2O (*dotted line*) emission as a function of radius, for the baseline disk model (see text) with $R_{in} = 3.0 \, R_\odot$ and $A_K = 2.05$. The dashed line shows the gas temperature of the line-emitting layer as a function of radius. The upper axis shows the value of $v \sin i$ corresponding to the radius on the lower axis.

H$_2$O, compared to CO (Bergin et al. 2003). In addition, the energetic X-rays emitted by T Tauri stars are a major source of ionization in the disk atmosphere (Glassgold, Najita, & Igea 1997; Igea & Glassgold 1999) that directly affect the chemical abundances (Aikawa & Herbst 1999, 2001; Glassgold & Najita 2001).

Preliminary modeling by Glassgold & Najita (2001) also shows that X-ray–induced heating and chemistry in the inner disk can produce a temperature inversion in the gas and a strong vertical chemical structure. Such a vertical structure would likely alter interpretations based on the simplistic uniform structure in our disk model. For example, the apparent low abundance of H$_2$O could arise if CO is present over a larger vertical column than H$_2$O, with H$_2$O found at larger depths and lower temperatures in the disk atmosphere. In order to sort out the thermal-chemical structure of the inner disk and to understand the processes that produce that structure, physical models that calculate both the radial and vertical structure of the atmosphere are needed.

Another alternative that could mimic a reduced abundance is a continuum opacity that is just sufficient to reduce, but not totally suppress, the line emission. Grains are not expected in thermodynamic equilibrium (Pollack et al. 1994) for the temperatures and densities in the H$_2$O emission layer. However, if small amounts of dust survived or were mixed into the upper atmosphere from lower disk layers, then sufficient opacity could be produced. This suggests that the details of grain evaporation, condensation, and transport are potentially important considerations for the measurement of molecular abundances.

An interesting result of the spectral modeling is the large local line broadening that is required to fit the CO band head. The near overlap of CO transitions near the $v = 2-0$ band head is the key that allows a separation of the local broadening from the macrobroadening. For the baseline disk model with a local Gaussian profile, the nonthermal velocity dispersion was 11 km s^{-1}. Acceptable fits were obtained for ξ between 7 and 15 km s^{-1} (with changes in Σ and $v \sin i$). These values are far larger than the thermal dispersion of 0.9 km s^{-1} for CO at 2500 K and larger than the sound speed of 5.2 km s^{-1}. The baseline model with a Lorentzian profile required $\xi = 3.2$ km s^{-1}. While the core of this Lorentzian profile is subsonic, supersonic motions still occur in the line wings.

Evidence for supersonic line broadening has also been presented for the accretion disks of cataclysmic variable stars. Horne et al. (1994) found that a velocity dispersion of $\sim$Mach 6 was required to fit the veil of Fe II absorption features that were attributed to intervening disk material in the eclipsing system OY Car. Supersonic broadening was also found for several cataclysmic variable star disks by Marsh & Dhillon (1997). Their method was not dissimilar to ours, in that it relied on the profile overlap of two close atomic lines; however, in their case the large line widths could potentially be produced by Stark broadening.

It is tempting to identify the local line broadening with turbulence in a disk. Turbulent motions in disks are believed to be closely linked to a long-standing difficulty in the understanding of accretion disk physics, namely, the physical process responsible for angular momentum transport in disks. Several possibilities have been suggested in the context of T Tauri disks. One attractive suggestion is the magnetorotational instability (Balbus & Hawley 1991; Stone et al. 2000), in which a weak magnetic field in a conducting, differentially rotating fluid renders it unstable to turbulence. More recently,

Klahr & Bodenheimer (2003) have proposed that the global baroclinic instability, a purely hydrodynamic instability, is a source of turbulence that leads to angular momentum transport in disks. Either of these processes could operate in the region probed by our observations ($r < 0.4$ AU); in particular, at the temperatures indicated by the modeling ($T > 1200$ K), thermal ionization is sufficient for the magnetorotational instability to be operative if a weak magnetic field is present. Both instabilities are expected to produce turbulent velocities that are less than or comparable to the sound speed. Simulations of these instabilities also show that the velocity dispersion increases with height in the disk, eventually reaching the sound speed (Klahr & Bodenheimer 2003; Miller & Stone 2000) in the upper disk atmosphere. The upper atmosphere of the disk is the region where we believe the CO and H$_2$O emission lines originate.

In our modeling, the fits with Gaussian local profiles would imply supersonic turbulence of $\sim$Mach 2. Models using a Lorentzian profile, however, show that it is possible to fit the CO band head using a profile that has a Gaussian core with a subsonic width, but stronger than Gaussian wings at high velocities. Hence, a non-Gaussian profile would allow the bulk of the motions to be transonic or subsonic and consistent with the velocities expected for turbulence in protoplanetary disks. In addition, non-Gaussian line profiles might be expected, given that a characteristic of turbulence seen in both laboratory experiments and numerical simulations are non-Gaussian wings in the probability density functions (PDFs) of the velocity (Frisch 1995; references cited in Falgarone et al. 1994). Indeed, it has been argued that evidence of turbulence in the interstellar medium is provided by the non-Gaussian high-velocity wings of molecular line profiles (Falgarone & Phillips 1990; Falgarone et al. 1994) and the non-Gaussian wings in the PDFs of centroid velocities or centroid velocity increments (Miesch & Scalo 1995; Lis et al. 1996, 1998; Miesch, Scalo, & Bally 1999).

If the local, nonthermal line broadening is due to disk turbulence, then analyses of other stars, and measurements of molecular transitions that probe different temperatures and radii, would be of great interest. Modeling of CO overtone emission by Najita et al. (1996) in two other YSOs also required large local velocity dispersions, although not quite as large as the broadening that we require for SVS 13. If large velocity dispersions are characteristic of the molecular-line–emitting regions of the inner disk, this may help to explain why centrally peaked, rather than double-peaked, profiles are commonly observed in the CO fundamental emission lines in T Tauri stars (Najita et al. 2003). Modeling of these CO fundamental lines can provide the magnitude of the local velocity dispersion. Our current data for SVS 13, unfortunately, do not allow an independent determination of ξ for H$_2$O, but this could be accomplished if some H$_2$O lines with the correct velocity separation can be identified and analyzed. In any case, further high-resolution spectroscopy and radiative transfer modeling of disk emission lines could provide observational evidence for the turbulence responsible for angular momentum transport in disks and supply information on both the magnitude and character of the turbulent motions (see, e.g., Horne 1995 on the possibility of detecting anisotropic turbulence).

A number of other YSOs with CO overtone emission show emission from hot H$_2$O (Najita et al. 2000). However, the current data are insufficient to say how common hot H$_2$O emission is among young stars. CO fundamental emission is commonly observed in T Tauri stars (Najita et al. 2003), and

the H_2O excitation temperature is closer to the typical temperature of the CO fundamental emission than to that of the overtone emission, which suggests that hot H_2O emission could be common. On the other hand, the total column densities deduced for the H_2O emission ($\Sigma \sim 1-10$ g cm^{-2}) are similar to those required for CO overtone emission and larger than those typical of fundamental emission ($\Sigma < 0.1$ g cm^{-2}); hence, the H_2O transitions that we have observed in SVS 13 may be too weak to measure in a typical T Tauri star. The stronger, lower excitation, H_2O transitions in the mid-infrared may be a more promising prospect for the study of water in protoplanetary disks. Because the rich spectrum of H_2O in the infrared could make water emission an effective probe of disks, further observations in both the near- and mid-infrared to determine the occurrence and characteristics of H_2O emission are warranted.

REFERENCES

Aikawa, Y., & Herbst, E. 1999, A&A, 351, 233
———. 2001, A&A, 371, 1107
Allard, F., Hauschildt, P. H., Alexander, D. R., Tamanai, A., & Schweitzer, A. 2001, ApJ, 556, 357
Allard, F., Hauschildt, P. H., & Schweitzer, A. 2000a, ApJ, 539, 366
Allard, F., Hauschildt, P. H., & Schwenke, D. 2000b, ApJ, 540, 1005
Aspin, C., & Sandell, G. 1997, MNRAS, 289, 1
Balbus, S. A., & Hawley, J. F. 1991, ApJ, 376, 214
Bergin, E., Calvet, N., D'Alessio, P., & Herczeg, G. J. 2003, ApJ, 591, L159
Brittain, S., Rettig, T. W., Simon, T., Kulesa, C., DiSanti, M. A., & Dello Russo, N. 2003, ApJ, 588, 535
Calvet, N., Patino, A., Magris, G., & D'Alessio, P. 1991, ApJ, 380, 617
Carr, J. 1989, ApJ, 345, 522
Carr, J. S., Mathieu, R. D., & Najita, J. R. 2001, ApJ, 551, 454
Carr, J. S., & Tokunaga, A. 1992, ApJ, 393, L67
Carr, J. S., Tokunaga, A. T., Najita, J., Shu, F. H., & Glassgold, A. E. 1993, ApJ, 411, L37
Chandler, C., Carlstrom, J., & Scoville, N. 1995, ApJ, 446, 793
Chandler, C. J., Carlstrom, J. E., Scoville, N. Z., Dent, W. R. F., & Geballe, T. R. 1993, ApJ, 412, L71
Falgarone, E., Lis, D. C., Phillips, T. G., Pouquet, A., Porter, D. H., & Woodward, P. R. 1994, ApJ, 436, 728
Falgarone, E., & Phillips, T. G. 1990, ApJ, 359, 344
Frisch, U. 1995, Turbulence: The Legacy of A. N. Kolmogorov (Cambridge: Cambridge Univ. Press)
Geballe, T. R., & Persson, S. E. 1987, ApJ, 312, 297
Glassgold, A. E., & Najita, J. R. 2001, in ASP Conf. Ser. 244, Young Stars Near Earth: Progress and Prospects, ed. R. Jayawardhana & T. Greene (San Francisco: ASP), 521
Glassgold, A. E., Najita, J., & Igea, J. 1997, ApJ, 485, 920
Greene, T. P., Tokunaga, A. T., Toomey, D. W., & Carr, J. S. 1993, Proc. SPIE, 1946, 313
Hauschildt, P. H., Allard, F., & Baron, E. 1999, ApJ, 512, 377
Henning, Th., & Stognienko, R. 1996, A&A, 311, 291
Herbig, G. H., & Jones, B. F. 1983, AJ, 88, 1040
Horne, K. 1995, A&A, 297, 273
Horne, K., Marsh, T. R., Cheng, F. H., Hubeny, I., & Lanz, T. 1994, ApJ, 426, 294
Igea, J., & Glassgold, A. E. 1999, ApJ, 518, 848

Irwin, A. 1988, A&AS, 74, 145
Jones, H. R. A., Pavlenko, Y., Viti, S., & Tennyson, J. 2002, MNRAS, 330, 675
Klahr, H. H., & Bodenheimer, P. 2003, ApJ, 582, 869
Leggett, S. K., Allard, F., Dahn, C., Hauschildt, P. H., Kerr, T. H., & Rayner, J. 2000, ApJ, 535, 965
Leggett, S. K., Allard, F., Geballe, T. R., Hauschildt, P. H., & Schweitzer, A. 2001, ApJ, 548, 908
Lis, D. C., Keene, J., Li, Y., Phillips, T. G., & Pety, J. 1998, ApJ, 504, 889
Lis, D. C., Pety, J., Phillips, T. G., & Falgarone, E. 1996, ApJ, 463, 623
Marsh, T. R., & Dhillon, V. S. 1997, MNRAS, 292, 385
Miesch, M. S., & Scalo, J. M. 1995, ApJ, 450, L27
Miesch, M. S., Scalo, J., & Bally, J. 1999, ApJ, 524, 895
Miller, K. A., & Stone, J. M. 2000, ApJ, 534, 398
Najita, J., Carr, J. S., Glassgold, A. E., Shu, F. H., & Tokunaga, A. T. 1996, ApJ, 462, 919
Najita, J., Carr, J. S., & Mathieu, R. D. 2003, ApJ, 589, 931
Najita, J. R., Edwards, S., Basri, G., & Carr, J. 2000, in Protostars and Planets IV, ed. V. Mannings, A. P. Boss, & S. S. Russell (Tucson: Univ. Arizona Press), 457
Partridge, H., & Schwenke, D. 1997, J. Chem. Phys., 106, 4618 (PS)
Pollack, J. B., Hollenbach, D., Beckwith, S., Simonelli, D. P., Roush, T., & Fong, W. 1994, ApJ, 421, 615
Rayner, J. T., Toomey, D. W., Onaka, P. M., Denault, A. J., Stahlberger, W. E., Vacca, W. D., Cushing, M. C., & Wang, S. 2003, PASP, 115, 362
Rothman, L., et al. 1998, J. Quant. Spectrosc. Radiat. Transfer, 60, 665
Scoville, N., Kleinmann, S. G., Hall, D. N. B., & Ridgway, S. T. 1983, ApJ, 275, 201
Sneden, C. 1973, Ph.D. thesis, Univ. Texas
Stone, J. M., Gammie, C. F., Balbus, S. A., & Hawley, J. F. 2000, in Protostars and Planets IV, ed. V. Mannings, A. P. Boss, & S. S. Russell (Tucson: Univ. Arizona Press), 589
Thompson, R. I. 1985, ApJ, 299, L41
Tokunaga, A. T., Toomey, D. W., Carr, J. S., Hall, D. N. B., & Epps, H. W. 1990, Proc. SPIE, 1235, 131
Vacca, W. D., Cushing, M. C., & Rayner, J. T. 2003, PASP, 115, 389
Wallace, L., & Livingston, W. C. 1992, An Atlas of a Dark Sunspot Umbral Spectrum in the Infrared from 1970 to 8640 cm^{-1} (Tucson: NOAO)
Zobov, N. F., et al. 2000, ApJ, 530, 994